JOC The Journal of Organic Chemistry

Featured Article

Dynamic Refolding of Ion-Pair Catalysts in Response to Different Anions

Antti J. Neuvonen, Dimitris Noutsias, Filip Topi#, Kari Rissanen, Tamás Földes, Imre Pápai, and Petri M. Pihko

J. Org. Chem., **Just Accepted Manuscript** • DOI: 10.1021/acs.joc.9b01980 • Publication Date (Web): 19 Sep 2019

Just Accepted

is published by the American Chemical Society. 1155 Sixteenth Street N.W., Washington, DC 20036

Dynamic Refolding of Ion-Pair Catalysts in Response to Different Anions

Antti J. Neuvonen,‡¶ Dimitris Noutsias,‡¶ Filip Topic,¶ Kari Rissanen,¶ Tamás Földes,† Imre Pápai,† Petri M. Pihko*¶

¶ Department of Chemistry and NanoScience Center, University of Jyväskylä, FI-40014 JYU, Finland

† Institute of Organic Chemistry, Research Centre for Natural Sciences, Hungarian Academy of Sciences, H-1117 Budapest, Magyar tudósok körútja 2, Hungary

Petri.Pihko@jyu.fi

‡ These authors contributed equally.

KEYWORDS catalysis, folding, anion binding, X-ray, solution structures, conformational change

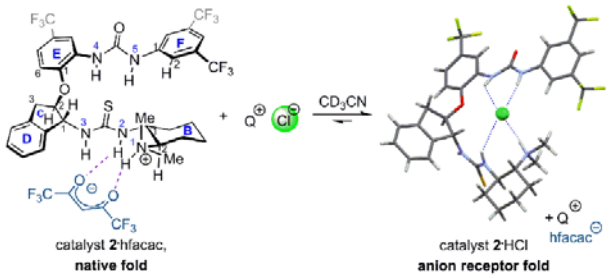

ABSTRACT: Four distinct folding patterns are identified in two foldamer-type urea-thiourea catalysts bearing a basic dimethylamino unit by a combination of X-ray crystallography, solution NMR studies, and computational studies (DFT). These patterns characterized by different intramolecular hydrogen bonding schemes that arise largely from different thiourea conformers. The free base forms of the catalysts are characterized by folds where the intramolecular hydrogen bonds between the urea and the thiourea units remain intact. In contrast, the catalytically relevant salt forms of the catalyst, where the catalyst forms an ion pair with the substrate or substrate analogues, appear in two entirely different folding patterns. With larger anions that mimic the dialkyl malonate substrates, the catalysts maintain its native fold both in the solid state and in solution, but with smaller halide anions (fluoride, chloride and bromide), the catalysts fold around the halide anion (anion receptor fold) and the intramolecular hydrogen bonds are disrupted. Titration of catalyst hexafluoroacetylacetonate salt with tetra-*n*-butylammonium chloride results in dynamic refolding of the catalyst from the native fold to the anion receptor fold.

INTRODUCTION

The prevailing tenet in designing enantioselective catalysts is that the catalyst must be able to efficiently differentiate between two competing diastereomeric transition states leading to different enantiomers of the product.[1] To this end, catalyst structures often include relatively bulky side chains to increase steric constraints[2] and to restrain conformational flexibility.

In contrast to the rigid design of synthetic catalysts, recent research has unearthed evidence that enzyme catalysis is highly tolerant of conformational *flexibility* in the structure of the protein.[3] In some cases, the binding of the substrate helps in preorganizing the active site of the enzyme.[4] It also appears that even after long periods of evolutionary optimization, enzymes often possess significant conformational flexibility that enables them to adapt to different substrates.[5] These properties are crucial for evolution of new functions and also for allosteric regulation. While the importance of conformational adaptability is well recognized in the realm of enzymes, conformational flexibility of synthetic catalysts has gained recognition only relatively recently.[6] In particular, synthetic peptides, in the same fashion as larger enzyme proteins, provide an important exception to the typical rigidity of synthetic catalysts. [6c-e]

Herein we describe a pair of highly enantioselective synthetic catalysts displaying significant conformational flexibility, with a native, active folded state and at least three alternative folded states.

The catalysts that are the subject of the current study (**1**-**3**, see Scheme 1) are capable of highly enantioselective catalysis of Mannich reaction between malonate esters, or β-keto esters, and imines.[7,8] The intramolecular urea-thiourea hydrogen bond motif in these catalysts was originally designed by the Smith group as a β-turn mimic,[9] connecting the design our catalysts to the realm of peptides. Mechanistically, an initial proton transfer event, the malonate or β-keto ester anions are proposed to be tightly bound

to the catalytic pocket via hydrogen bonds (Scheme 1 a).[7a] While all catalysts gave reasonable enantioselectivities in the catalytic Mannich reaction (Scheme 1 b), catalyst **1** was superior to catalyst **2** in both selectivity as well as reactivity (Scheme 1 b),[7d] and catalyst **3** was even more selective than either catalysts **1** or **2**. We have earlier reported[7a] how important the catalytic pocket and the overall fold, including the rigid indane ring[7c] (rings C and D), are for catalysis with this catalyst family (Scheme 1 c).

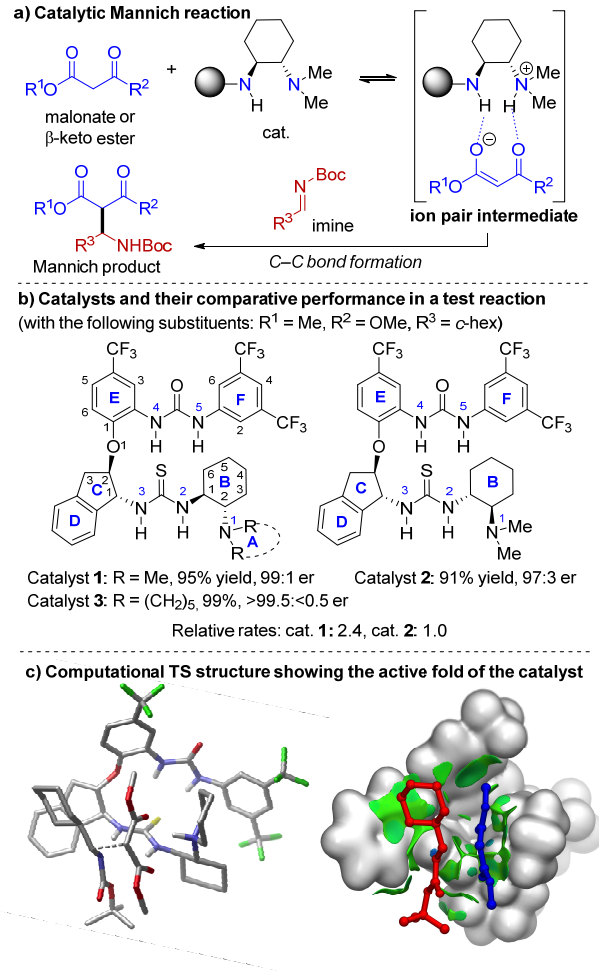

Scheme 1. a) The catalytic Mannich reaction via ion-pair intermediate, b) structures of catalysts **1**-**3** and their relative performance in a test reaction (10 mol% catalyst, toluene, 0 °C for catalysts **1** and **3**, –40 °C for **2**, see ref. 7a and 7c) and c) transition state (TS) structure(DFT) showing catalyst **3** and the test substrates, showing the folding of the catalyst in the TS (left) and the surface of the active site cleft (right)[7a].

However, evidence for alternative folds with these catalysts was evident even in our first X-ray studies. For example, a completely different type of fold was characterized by X-ray when the counter anion was a small chloride ion (Figure 1). In this case, the intramolecular hydrogen bonded fold and the catalytic cleft was completely disrupted and the catalyst instead folded around the chloride ion.

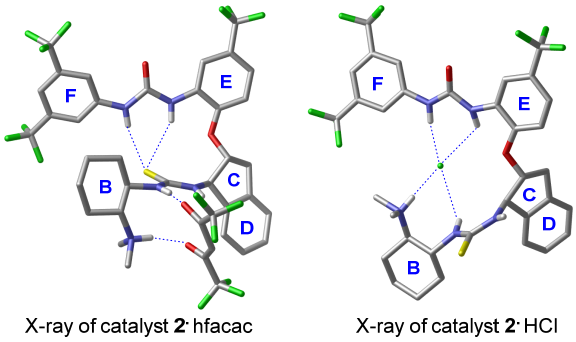

Figure 1. Two examples of previously characterized folding patterns of catalyst **2** (CCDC codes YEKPEL and YEKPIP) in their active, salt form.[7c]

The presence of several different folds in catalysts is well established in the realm of enzymes, where it is possible to distinguish between the native, catalytically competent state, and other, improperly folded or even denatured states.[5] Our foldamer-like catalysts, are complex enough that different folding patterns may similarly emerge. These folding patterns, or folds, arise as a combination of four possible conformations for the thiourea unit (Figure 2 a)[10] and the presence of hydrogen bond acceptors and donors within the catalyst, giving rise to additional conformational possibilities. Some of the possible folding patterns are shown in Figure 2 b. Fold **A** is the fold that we have previously associated with catalytic activity,[7a,7c] exhibiting the *anti-anti* thiourea unit and intramolecular urea-thiourea hydrogen bonds. Given its potential role in catalysis, fold **A** is herein called the "native fold", whereas the chloride-disrupted fold **D** is called "anion receptor fold".[11]

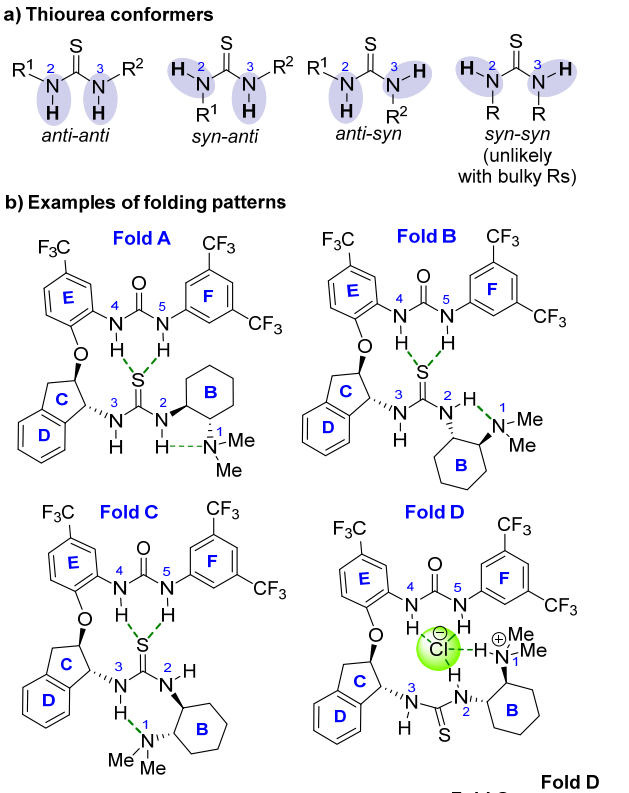

	Fold A ("native")	Fold B	Fold C	Fold D "anion receptor"
Thiourea conformation	*anti-anti*	*syn-anti*	*syn-anti*	*anti-syn*
Urea-thiourea HBs	*yes*	*yes*	*yes*	*no*
N2–H···NMe_2 HB	*yes*	*yes*	*no*	*no*
N3–H···NMe_2 HB	*no*	*no*	*yes*	*no*

Figure 2. a) Different thiourea conformations with unsymmetrical thioureas and b) possible folding patterns in catalyst **1**.

Our early studies, however, did not establish to what extent the native fold of these catalysts was maintained in solution. Furthermore, why did the chloride anion give rise to the anion receptor folding pattern, while the hexafluoroacetylacetonate (hfacac) anions maintained the native fold of the catalyst? In order to study the behavior of the catalysts in a more systematic manner, we decided to examine the original catalysts **1** and **2,** and their salts with different anions, both in solution and in the solid state. The free catalysts were examined first, followed by a more systematic variation of different anions, from small halides to larger organic anions mimicking possible pronucleophiles.

RESULTS AND DISCUSSION

Improved Synthesis of Catalysts 1 and 2. We have found that the precursor **4** (Scheme 2) is hindered enough to enable a straightforward and highly selective monothiourea formation between **4** and **5** (via a isothiocyanate derived from **4**). In this manner, catalysts **1** and **2** can be obtained very easily from precursor **4** after reductive amination of intermediate **6** or **7.**

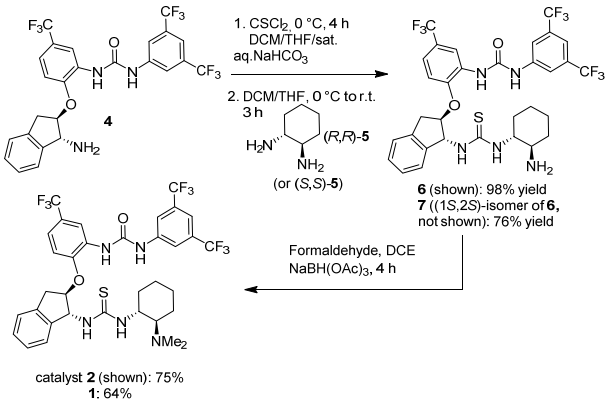

Scheme 2. Improved synthesis of catalysts **1** and **2** directly from diamine 5.

Solid-state Structures of Free Catalysts 1 and 2. The X-ray structures of the free catalysts **1** and **2** were published previously.[7c] For comparison, the salient features of the structures are discussed herein.

Catalyst **1** exhibits the native folded conformation **1A** in the X-ray structure (Figures 3 and 4). In this structure, the thiourea sulfur atom is hydrogen bonded to the urea H_{N5}. The distance from the thiourea sulfur to N_5 was 3.29 Å (H_{N5}···S distance 2.48 Å)[12]. In turn, the hydrogen bond from thiourea sulfur to the second urea H_{N4} was weaker, with S···N_4 distance of 3.51 Å (H_{N4}···S 2.68 Å). The differentiation between the two urea H-bond donors is mainly caused by geometrical restraints from the aminoindanol linker and limited rotation around the ether bonds due to 1,5-interaction. In this structure, the angle between least squares planes of the urea and thiourea is 75.8°. The thiourea unit is in the catalytically active (*anti-anti*) conformation, with the N_2-H and N_3-H bonds parallel, facing outwards and open for coordination by hydrogen bond acceptors. The H_{N2}–N_2–C_{B1}–H_{B1} and H_{N3}–N_3–C_{C1}–H_{C1} dihedral angles on both sides of the thiourea are governed by allylic strain by minimizing the interaction between sulfur and the neighboring alkyl groups. This conformation is analogous to highly preferred 120° or 180° φ-angle clusters in peptides.[13] In fact, in catalyst **1**, torsion angle of H_{N2}–N_2–C_{B1}–H_{B1} is close to 120° (133°) and the torsion angle of H_{N3}–N_3–C_{C1}–H_{C1} is close to 180° (169°) (Figure 3). The thiourea hydrogens H_{N2} and H_{N3} form intermolecular hydrogen bonds to urea oxygen of the adjacent catalyst molecule with hydrogen bond lengths 3.00 Å (N_2···O') and 2.99 Å (N_3···O') (H···O' distance being 2.17 Å for both hydrogen bonds).

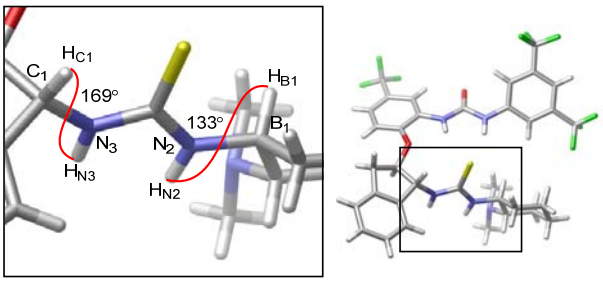

Figure 3: φ-angle torsions in (*anti-anti*) conformer of solid-state structure of catalyst **1**.

In contrast to the free catalyst **1**, the X-ray structure of catalyst **2** shows two crystallographically independent conformations, **2B** and **2C** (Figure 4). Fold **2A** was not observed in the solid state. In both

conformations (**2B** and **2C**), the catalyst backbone stays relatively unchanged, highlighting its rigidity. However, the folding of the rest of the catalyst is different from the fold **1A** observed for **1** (Figure 4). In both **2B** and **2C**, the thiourea is the *syn-anti* conformer, and the intramolecular hydrogen bonds between the urea and thiourea units are retained. The difference between **2B** and **2C** lies in the orientation of cyclohexyl ring B. In **2B**, the dimethylamino group (N_1) can form one more intramolecular hydrogen bond with the thiourea H_{N2} ($N_2 \cdots N_1$ distance 2.70 Å and $H_{N2} \cdots N_1$ distance 2.37 Å), but in **2C**, a similar contact is not possible. A weaker hydrogen bond between N_1 and H_{N3} is feasible based on the $N_3 \cdots N_1$ distance, 3.03 Å and $H_{N3} \cdots N_1$ distance of 2.56 Å.

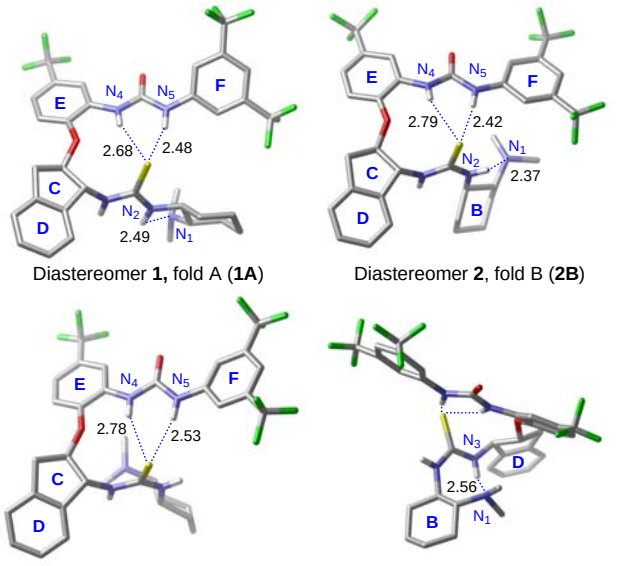

Diastereomer **1,** fold A (**1A**) Diastereomer **2**, fold B (**2B**)

Diastereomer **2**, fold C (**2C**) Diastereomer **2**, fold C (**2C**), back view

Figure 4. The X-ray structures of diastereomers **1** (CSD: YEKQEM) and **2** (YEKPAH) showing three distinct folds for the catalysts. All except NH hydrogens are omitted for clarity.

Solution Structures of Free Catalysts 1 and 2. The observation of three distinct folds in these X-ray structures supported the notion that these catalysts can adopt a variety of conformations in the solid state. The catalytic reactions, however, take place in solution. To assess the solution conformations, NOESY NMR spectra of the catalysts **1** and **2** were recorded in CD_2Cl_2. Different conformations of the catalysts **1** and **2** were also examined computationally. We used DFT calculations at the M06-2X/6-311++G(3df,3pd)//M06-2X/6-311G(d,p) level to compute the structure and the relative stability of various catalyst conformers (for details, see Supporting Information).

The most stable computed structures are shown in Figure 5 b and d. For catalyst **1**, three conformers with very similar relative stabilities were identified. Conformer **1A** displays the conformation observed in the X-ray structure of **1**, with the *anti-anti* thiourea. The conformers **1B** and **1C**, in contrast, possess a *syn-anti* thiourea unit, but still involving intramolecular H-bonding interactions between the thiourea S atom and the urea NH groups. Neither of these folds were observed in the X-ray studies of **1**, but the **1B** fold is similar to the fold **2B** of catalyst **2**. For catalyst **2**, the most stable form corresponds to conformer **2B** displaying a *syn-anti* thiourea unit, whereas the *anti-anti*-thiourea conformation (**2A**) is predicted to be 1.5 kcal/mol less favored in free energy. The overall fold of **2B** in the X-ray structure is almost identical with the DFT structure (see Figure 5b). Interestingly, although fold **2C** was present in the X-ray structure (see above), it turned out to be 3.0 kcal/mol less stable than **2B**, even after optimization of the structure. The existence of fold **2C** in the X-ray crystal structure (Figure 4) may be attributed to intermolecular hydrogen bonds between the structures **2B** and **2C** in the X-ray structure (Figure 5 f). These hydrogen bonds could stabilize **2C** in the solid state.

In solution, the most diagnostic NOESY cross-peaks in catalyst **1** were those observed between N_1-Me$\leftrightarrow H_{C2}$, $H_{B1}\leftrightarrow H_{N5}$ and $H_{B1}\leftrightarrow H_{N4}$. The observed N_1-Me$\leftrightarrow H_{C2}$ interaction is consistent with the structures **1C** (computed distance 2.3 Å) and possibly also with **1A** (5.1Å), but appears inconsistent with the most stable conformer **1B** (6.1Å). The $H_{B1}\leftrightarrow H_{N5}$ interaction can be also supported by conformers **1A** (2.5 Å) and **1C** (3.5 Å), but the distance in **1B** is longer (4.8 Å). Last, the interaction between $H_{B1}\leftrightarrow H_{N4}$ is expected on the basis of structure **1A** (computed distance 3.8 Å) and **1C** (3.1 Å), but appears less likely for conformer **1B** (5.0 Å). Taken together, these results suggest that catalyst **1** is mostly populated by conformers **1A** and **1C** in the solution state, but we cannot rule out the contribution of conformer **1B** to the solution structure. The $\Delta G^{\ddagger}$ for the rotation around the thiourea C–N bond is 13.5-14.4 kcal/mol,[14] and as such NMR experiments at 303 K probe temperature used herein are well above the coalescence temperature.[14a]

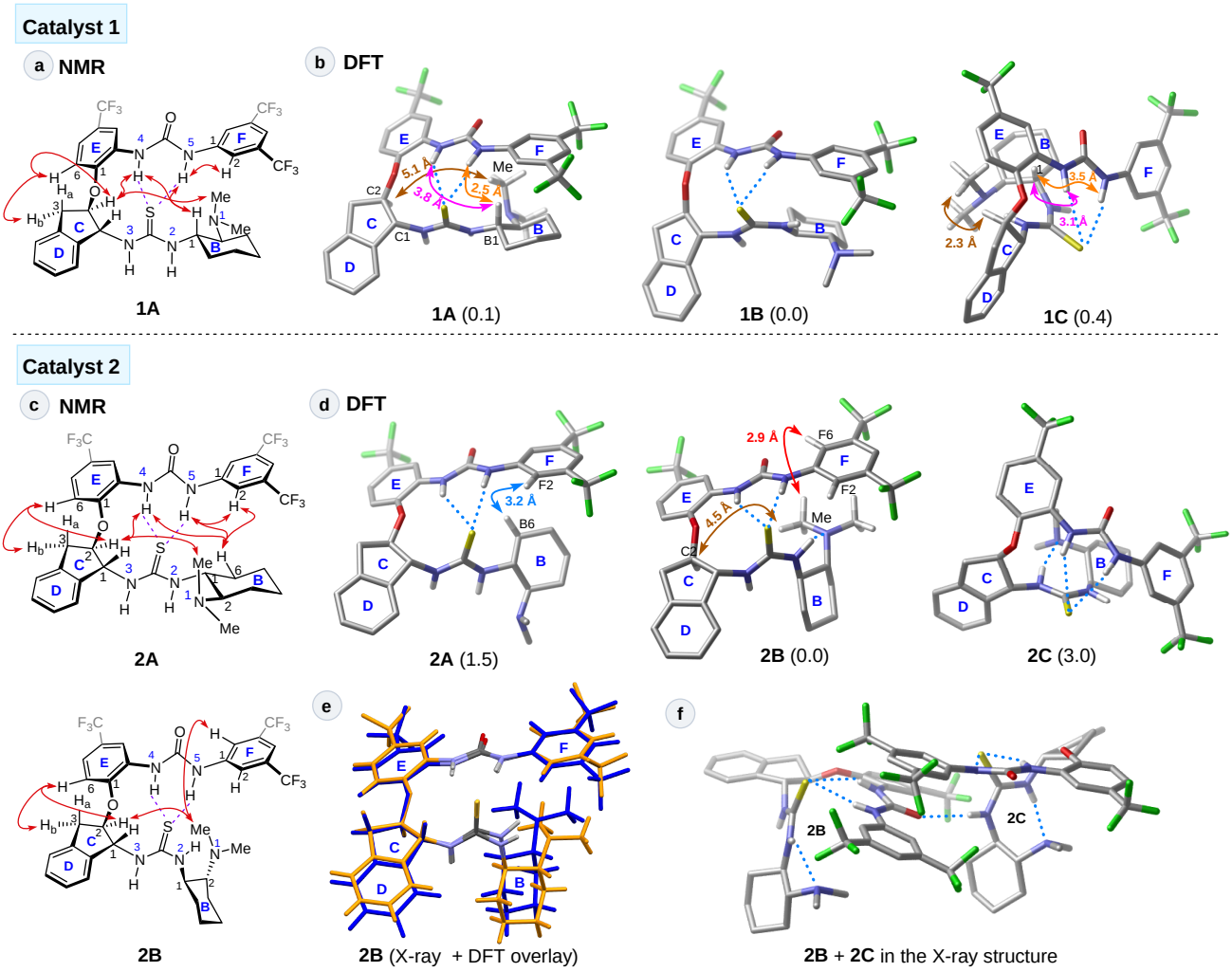

Figure 5. a-d) Key NOESY correlations (NMR) and the most stable DFT structures of free catalysts **1** and **2.** To rationalize the NMR results for catalyst **2**, two different folds (**2A** and **2B**) are presented to account for the observed NOESY cross-peaks (see text). e) Overlay of the X-ray of fold **2B** (gold) with the DFT structure (blue). f) Packing of structures **2B** and **2B** in the X-ray structure of **2** (CSD: YEKPAH). The computed relative stabilities shown in parenthesis (in kcal/mol) refer to solution phase Gibbs free energies with respect to the most stable forms of catalysts **1** and **2.**

In catalyst **2,** the key diagnostic NOESY cross-peaks correspond to the correlations between N_1-Me↔H_{C2}, H_{B6eq}↔$H_{F2/F6}$ and the N_1-Me↔$H_{F2/F6}$. The most stable DFT structures, **2A** and **2B**, are consistent with most of the observed NOESY cross-peaks. The N_1-Me↔H_{C2} correlation is readily explained by fold **2B** (computed distance 4.5 Å), but not by **2A** (Me_{N1}···H_{C2} distance 6.7 Å). Likewise, the correlation N_1-Me↔$H_{F2/F6}$ is expected for **2B** (2.9 Å) but the corresponding computed distance in **2A** is 5.4 Å. In contrast, the correlation H_{B6eq}↔$H_{F2/F6}$ cannot be readily rationalized by fold **2B** (distance 7.3 Å) but it is well consistent with **2A** (distance 2.9 Å). These data suggest that in solution, both folds, **2A** and **2B,** may contribute to the averaged NMR structure since neither of these structures alone can fully rationalize the observed NOEs.

Structures of the Halide Salts in the Solid State and in Solution. We decided to probe the effect of anion size by generating a series of structures from two available catalyst diastereomers with hydrohalic acids. Indeed, we could successfully form salts and isolate good quality single crystals of hydrofluoric, hydrochloric and hydrobromic acid salts of both catalysts **1** and **2**. Salts of hydroiodic acid, however, did not afford crystalline material with either catalyst diastereomer.

The X-ray structures (Figure 6) show that the structures of the hydrohalide salts are remarkably similar with different anions. In all structures, the halide anions are bound to the catalyst **1** via the urea H_{N4} and H_{N5} hydrogens and via one of the thiourea NH, the H_{N2}. The thiourea is in the *anti-syn* conformation.[15] The protonated ammonium H_{N1} forms a weaker hydrogen bond to the halide with a longer H···N distance. For example, in **1**·HF the H_{N1}···F distance is 2.54 Å (N_1···F 3.10 Å), while the contacts to the thiourea and urea protons are shorter (H_{N2}···F 1.93 Å, H_{N4}···F 2.08 Å, H_{N5}···F 1.87 Å). In addition, the fluoride ion also contacts the thiourea H_{N3} of the adjacent catalyst molecule in the solid state structure (see the SI).[16]

All catalyst **1** halide salts show a similar bonding pattern, and the catalyst molecules overlap almost perfectly. Although the binding of the halide causes a small distortion in the upper CDEF urea segment of the catalyst molecule, the overlaid structures of the free catalyst **1** and **1**·HCl show remarkable degree of similarity (Figure 6 e).

The X-ray crystal structures of the hydrohalide salts of catalyst **2** are also remarkably similar to the HX salts of catalyst **1**. The only major change in the folding pattern is that the dimethylammonium group in this diastereomer is better able to contact the halide ion, even in the case of the smallest, fluoride anion (see Figure 6 b). In contrast, the thiourea H_{N2} is not ideally pointed towards the halide ion, and forms only a weak contact with the anion, with a $H_{N2}\cdots F$ distance of 2.96 Å in **2**·HF (Figure 6 b).

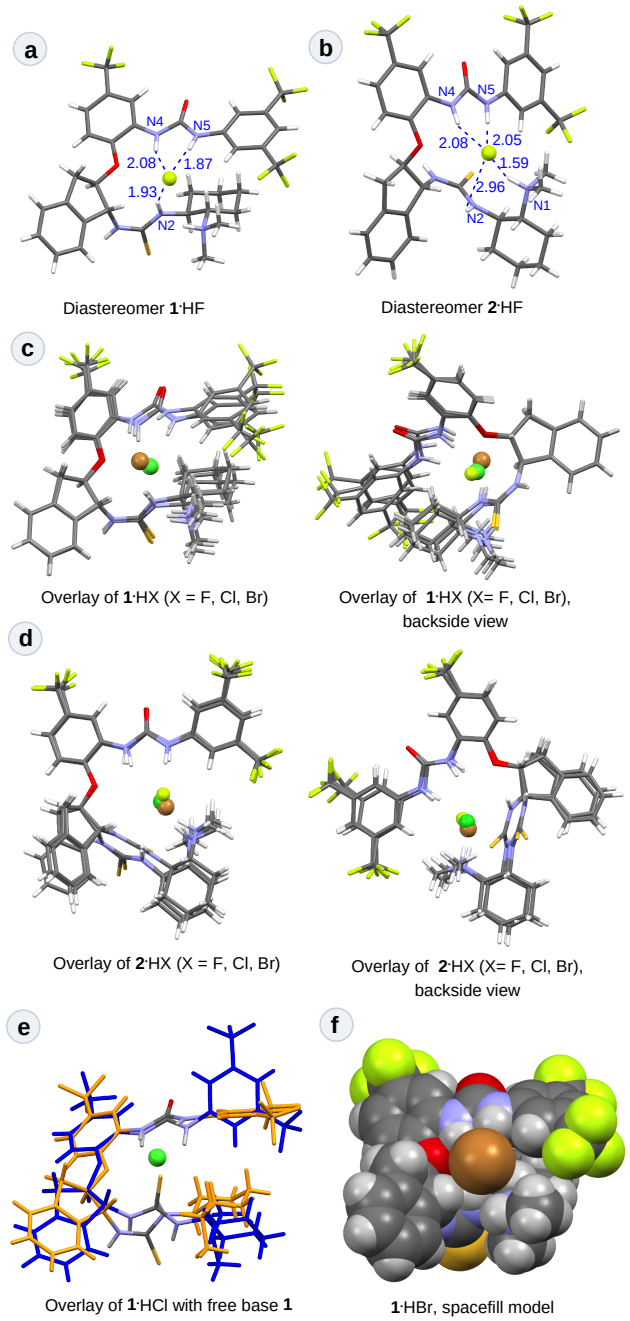

Figure 6. a-d: Solid state structures of the HX salts of catalysts **1** and **2**. e) Overlay of the X-ray structures of **1**·HCl (blue, except for the urea and thiourea units) and free catalyst **1** (YEKQEM, gold) showing the similar folding of the CDEF region of the catalyst. f) Spacefill model of **1**·HBr showing how the bromide ion protrudes out from the binding pocket.

It is evident from these solid state structures that the halides do not fit the pocket perfectly and thus allow the formation of intermolecular hydrogen bonds on the exposed face of the anion. In particular, the bromide ion is large enough that it is bound only from one side of the sphere by one catalyst molecule, as exemplified by the spacefill structure of **1**·HBr (Figure 6 f).

Structures of Catalyst Hydrochloride salts: Solution State Structures. The NOESY spectrum of the HCl salt of catalysts *ent*-**1**[17] and **2** confirms most of the expected interactions that are observed in the X-ray structure (Figure 7). Many of the NOESY correlations observed in the free catalysts remained similar in the HCl salts. However, the correlation between H_{N2} and H_{C1} indicates a conformational change in the thiourea moiety to the *anti-syn* conformation. Furthermore, the cross-peaks between Me_{N1} and H_{F2} in both structures as well as H_{N5} and H_{B2} in *ent*-**1**·HCl were indicative of a folded, compact conformation where the catalyst wraps around the chloride ion.

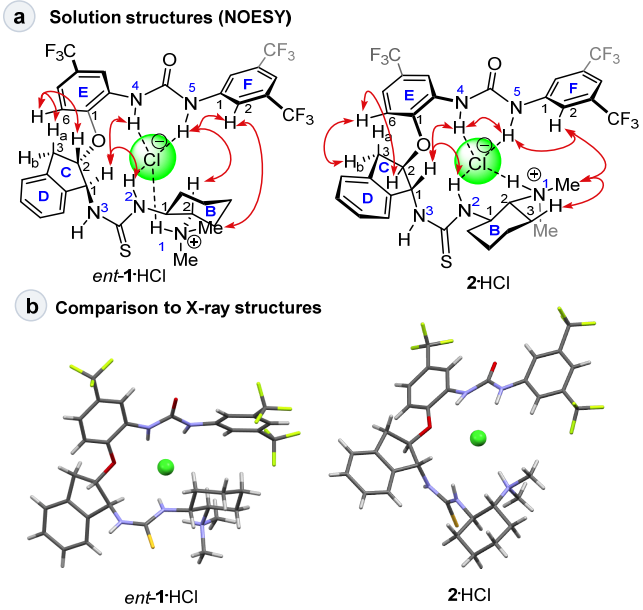

Figure 7. Structures of HCl salts of catalysts *ent*-**1** and **2** in a) CD_3CN (with diagnostic NOESY cross-peaks indicated by arrows) and b) in the solid state (X-ray). For the structure of *ent*-**1**·HCl, the mirror image of the X-ray of **1**·HCl is shown for clarity.

Structures of Catalyst with Organic Acids. In contrast to the salts of hydrohalic acids, we had already previously recorded examples where catalysts **1**-**3** exhibited the native fold **A** in the presence of organic acids.[7c] We therefore examined a series of acids with catalysts **1** and **2** to obtain further insight how the size and the shape of the anions affect the overall fold of the catalyst.

Although it would have been desirable to obtain X-ray structures for a complete series of anions, in practice these studies had to be limited to scattered cases where the crystal properties were satisfactory. In many cases, even if proper size crystals were obtained, they were often soft or brittle making the experiments hard to conduct. Nevertheless, in addition to the previously characterized **2**·hfacac (Figure 1), we could also obtain the corresponding trifluoroacetate (TFA, Figure 8 a), diphenylphosphate (DPP, Figure 8 b) and bis(2,6-trifluoromethyl)benzoate (BTB, see SI) salts, all of which exhibited the expected native fold **A**. The intermolecular hydrogen bonding

patterns observed in these structures are, however, dependent on the hydrogen bond acceptor properties of the anion. For example, in the DPP salt, the ammonium H_{N1} contacts a neighboring diphenylphosphate anion in the solid state (see the SI) instead of forming a third hydrogen bond to the anion that is bound by the urea. For these reasons, these X-ray structures may not always offer a realistic insight into the conformers populated in solution.

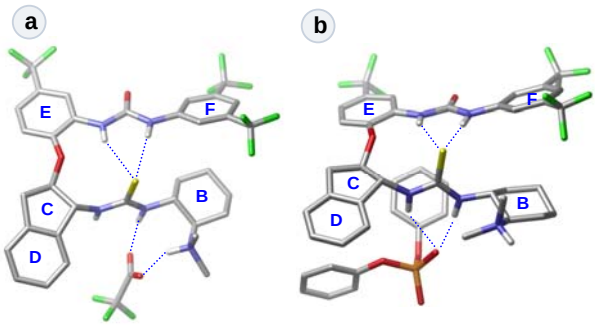

Figure 8. Solid state structures of catalyst **2** as the a) TFA salt and b) DPP salt.

Structures of Catalyst -hfacac Salts: Solution State Structures. The solution state structures of the hfacac salts of catalysts **1** and **2** were obtained by recording NOESY spectra in CD_2Cl_2 and analysis of the key correlations. The results (Figure 9) support the notion that these catalysts primarily populate fold **A** in solution with larger anions such as hfacac and the enolate of dimethyl malonate.[7a] For example, the $H_{N3} \leftrightarrow H_{C2}$ NOESY cross-peak observed in **1**·hfacac shows that the thiourea moiety is likely to adopt an *anti-anti* configuration. Most diagnostically, the cross-peaks between H_{F2} and H_{B2} and H_{B4ax} (**1**·hfacac) or H_{F2} and H_{5ax} (**2**·hfacac) are consistent with fold **A** (Figure 9).

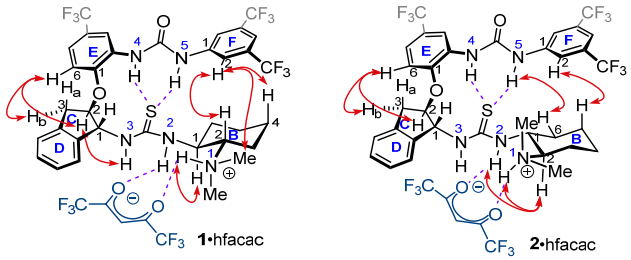

Figure 9. Solution state structures of hfacac salts of catalysts **1** and **2**.

Interestingly, the lower reactivity and selectivity of catalyst **2** relative to **1** may be related to its relatively lower preference for the active *anti-anti* conformer (fold **A**). Catalyst **2** will need to adopt the active fold **2A** instead of the preferred folds **2B** or 2**C** (with a *syn-anti* thiourea unit) upon binding to the malonate ion.[7a,7c] In contrast, catalyst **1** appears to populate the native fold **1A** with greater occupancy in solution (see Figure 4a). If fold **A** is the fold required for catalysis, this difference may explain the higher reactivity and selectivity of catayst **1** compared to **2**.

Addition of Chloride Ion Source Dynamically Switches the Catalyst Conformation in Solution. We also hypothesized that the refolding of the catalyst in the presence of different anions might be sufficiently rapid so that the event could be monitored by NMR. To this end, we selected *n*-Bu_4NCl as the chloride anion source that could potentially replace the hfacac anion in solution (Scheme 3).

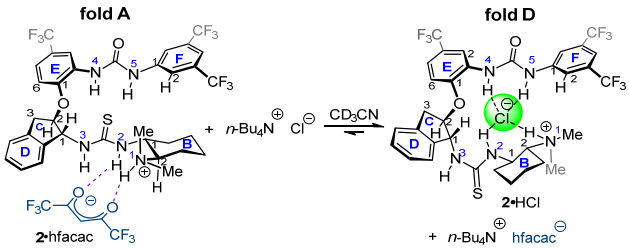

Scheme 3. Dynamic switching between the **A** and **D** folds of the catalyst with addition of *n*-Bu_4NCl as the chloride source.

Thus, a solution of **2**·hfacac in CD_3CN was titrated with a solution of *n*-Bu_4NCl (0.5 M in CD_3CN). During the titration, the ^1H NMR of the mixture slowly began to resemble the spectrum of pure **2**·HCl (compare Figures 10a and 10b), and only very little change was detectable beyond 1.2 equiv of *n*-Bu_4NCl (Figure 10 c). These data suggest that during the titration, catalyst **2** had almost exclusively switched from the fold **2A** to the anion receptor fold **2D**. Similar results were obtained with catalyst **1** and *n*-Bu_4NCl (see the SI for details). The titration results with *n*-Bu_4NCl point indicate that the equilibrium in this case lies on the side of the chloride complexes (D fold). However, titration of a solution of **2**·hfacac with *n*-Bu_4NBr (a source of bromide ion) yielded a more complex NMR spectrum, suggesting that in this case the switch was either not complete or that other conformations were also populated.

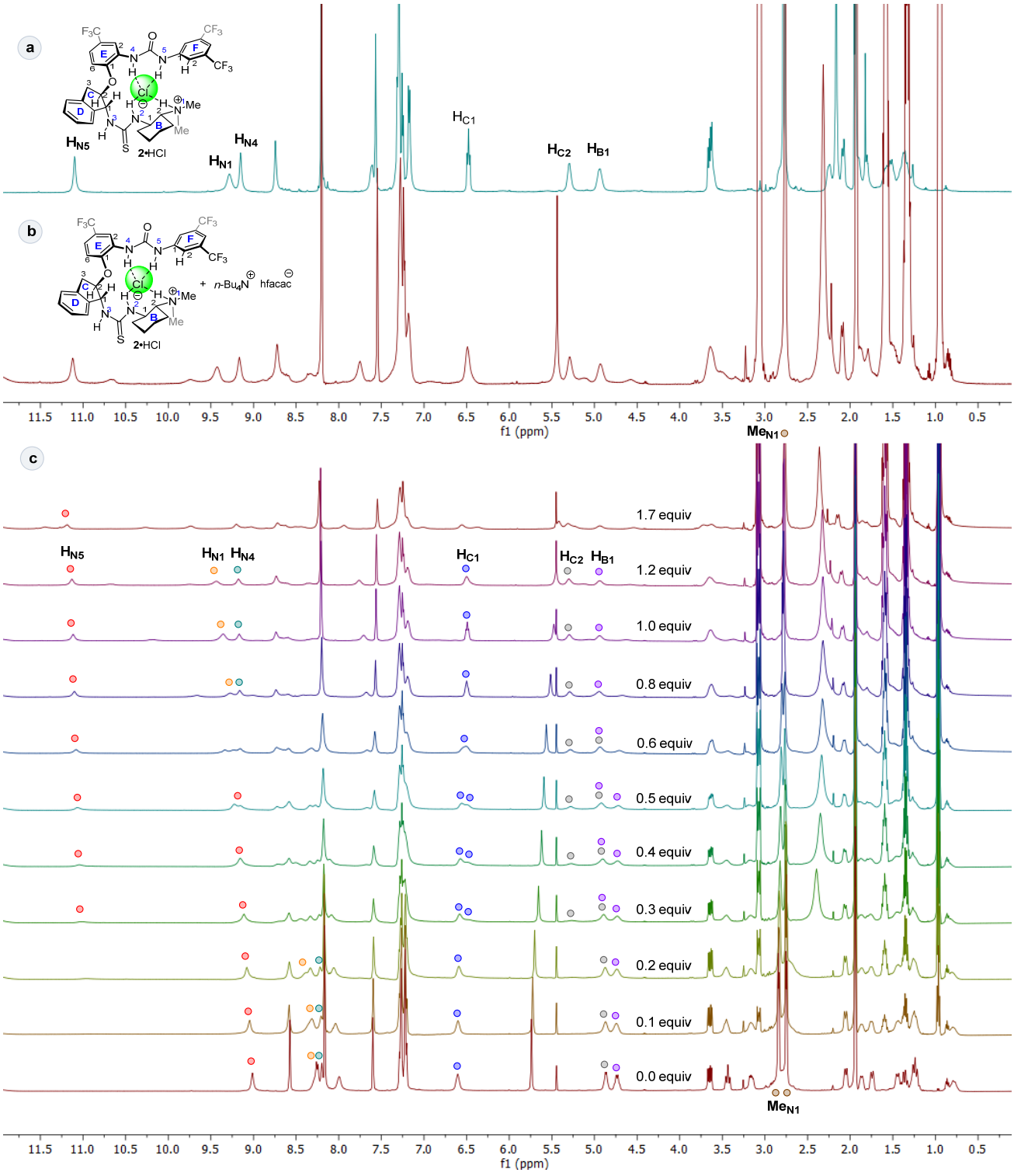

Figure 10. a) ^{1}H NMR spectrum of **2**·HCl. b) ^{1}H NMR spectrum of **2**·hfacac after addition of 1.2 equiv of *n*-Bu$_4$NCl. c)^{1}H NMR titration of **2**·hfacac with 0.5 M solution of *n*-Bu$_4$NCl. All spectra were recorded in CD_3CN.

SUMMARY AND CONCLUSIONS

In conclusion, the folding patterns of our foldamer-type catalysts, capable of highly enantioselective Mannich reactions have been characterized. The patterns that emerge from the solid-state XRD studies appear to be preserved in solution in high fidelity. Thus, the intramolecular hydrogen bonds in the native fold of the catalyst, where the catalytic pocket is intact, was maintained in the free base form of the catalyst as well as in its hfacac or TFA salts. However, the thiourea unit of the catalyst does not uniformly adopt the desired *anti-anti* conformation, and it turned out that the less-reactive catalyst **2** favoured the undesired *syn-anti* thiourea

conformer in solution, as established by a combination of NMR studies and computational conformational analysis.

In contrast, the salts with simple hydrohalic acids adopt a different, anion-receptor type fold, where the intramolecular hydrogen bonding is completely disrupted, and the catalyst conformation changes to allow multiple hydrogen bond contacts with the small halide counteranion. This fold is made possible by the alternative *anti-syn* conformation of the thiourea unit, instead of the *syn-anti* conformation observed for catalyst **2**. These folding patterns were identified by X-ray structures in the solid state for both catalyst diastereomers, and for different anions (F^-, Cl^-, and Br^-) and the hydrochloride salts of two catalyst diastereomers were found to populate similar conformations in solution according to NOE studies.

The choice of the fold could also be modulated by addition of chloride ions. Titration of the hfacac salts of the catalysts **1** and **2**, possessing the native fold in solution, with a chloride source (*n*-Bu_4NCl), resulted in a switch to the anion receptor mode as observed by ^1H NMR. The fact that different anions can affect the shapes of the catalysts suggests that anions could also be used to modulate the selectivities and activities of synthetic catalysts. Studies towards these goals are ongoing.

EXPERIMENTAL SECTION

General Information. All reactions were carried out under an argon atmosphere in flame-dried glassware, unless otherwise noted. When needed, nonaqueous reagents were transferred under argon *via* syringe or cannula and dried prior to use. THF and CH_2Cl_2 were obtained by passing deoxygenated solvents through activated alumina columns (MBraun SPS-800 Series solvent purification system). Other solvents and reagents were used as obtained from supplier, unless otherwise noted. Analytical TLC was performed using Merck silica gel F_{254} (230-400 mesh) plates and analyzed by UV light or by staining upon heating with anisaldehyde solution (2.8 mL anisaldehyde, 2 mL conc. H_2SO_4, 1.2 mL conc. CH_3COOH, 100 mL EtOH), vanillin solution (6 g vanillin, 5 mL conc. H_2SO_4, 3 mL glacial acetic acid, 250 mL EtOH) or $KMnO_4$ solution (1 g $KMnO_4$, 6.7 g K_2CO_3, 1.7 mL 1M NaOH, 100 mL H_2O). For silica gel chromatography, the flash chromatography technique was used, with Merck silica gel 60 (230-400 mesh) and p.a. grade solvents unless otherwise noted.

The ^1H NMR and ^{13}C NMR spectra were recorded in CD_2Cl_2 or CD_3CN on Bruker Avance 500, 400 or 250 spectrometers. The chemical shifts are reported in ppm relative to CHD_2CN (δ 1.94) or $CHDCl_2$ (δ 5.32) for ^1H NMR. For the ^{13}C NMR spectra, the residual CD_3CN (δ 118.26) or CD_2Cl_2 (δ 53.84) were used as the internal standards. The enantiomeric excesses (ee) of the products were determined by HPLC in comparison to the corresponding racemic samples using Waters 501 pump and Waters 486 detector. Melting points (mp) were determined in open capillaries using Gallenkamp melting point apparatus. IR spectra were recorded on a Tensor27 FT-IR spectrometer. Optical rotations were obtained with a Perkin-Elmer 343 polarimeter. High resolution mass spectrometric data were measured using MicroMass LCT Premier Spectrometer.

Single crystal X-ray diffraction analyses were performed at indicated measuring temperature on an Agilent Super-Nova diffractometer using mirror monochromatized Mo-*Kα* (λ = 0.71073 Å) or Cu-*Kα* (λ = 1.54184 Å) radiation. CrysAlisPro program was used for the data collection and processing. The intensities were corrected for absorption using the Analytical face index absorption correction method. The structure was solved by charge flipping method with SUPERFLIP5 and refined by full-matrix least-squares methods using the OLEX2-1.2 software, which utilizes the SHELXL module. All non-hydrogen atoms were refined with anisotropic thermal parameters. Hydrogen atoms were introduced in proper positions with isotopic thermal parameters using the 'riding model'. ORTEP figure was plotted and structure was analyzed with Mercury v 3.10.

Synthesis of Catalysts. CAUTION: $CSCl_2$ (thiophosgene) is a toxic and corrosive reagent that must be used in an efficient fume cupboard.

1-(2-(((1R,2R)-1-(3-((1R,2R)-2-aminocyclohexyl)thioureido)-2,3-dihydro-1H-inden-2-yl)oxy)-5-(trifluoromethyl)phenyl)-3-(3,5-bis(trifluoromethyl)phenyl)urea (**6**). Amine **4** (430 mg, 0.76 mmol, 100 mol-%) was dissolved in a stirred biphasic mixture of DCM, THF and saturated aqueous $NaHCO_3$ (10:1:10, total volume 21 mL) at 0 °C. The stirring was stopped and thiophosgene (117 μL, 1.52 mmol, 200 mol-%) was added *via* syringe to the organic layer. Stirring was started and continued for 4 h at 0 °C after which the layers were separated and the aqueous layers extracted with DCM (3 × 20 mL). The combined organic extracts were dried over Na_2SO_4 and concentrated. The crude isothiocyanate was dissolved in a mixture of dry DCM, THF (5:1, total volume 12 mL) under argon and diamine (*R,R*)-**5** (174 mg, 1.52 mmol, 200 mol-%) was added in one portion at 0 °C. The reaction mixture was stirred at rt for 3 h after which most of the solvents were removed under reduced pressure (2 mL of solvent left in the flask). Purification of the residue by flash chromatography (100:1:1 DCM:MeOH:Triethylamine) afforded the desired product **6** as off-white solid (535 mg, 98%). R_f (4% 7N NH_3/MeOH in DCM) = 0.35; mp 141−142 °C; $[\alpha]_D^{25\,°C}$ = −50.7 (*c* 1.0, CH_2Cl_2); IR (film, cm¬1): 3259, 3083, 2934, 2860, 1709, 1543, 1385, 1276, 1170, 1121, 681; ^1H NMR (500 MHz, CD_2Cl_2): δ 10.25 (s, 1H), 9.21 (s, 1H), 8.69 (s, 1H), 8.67 (brs, 1H), 8.17 (s, 2H), 7.53 (s, 1H), 7.34 – 7.30 (m, 4H), 7.25 (d, *J* = 8.4 Hz, 1H), 7.05 (d, *J* = 8.4 Hz, 1H), 6.64 (brs, 1H), 6.13 (brs, 1H), 4.61 (app q, *J* = 8.2 Hz, 1H), 3.66 (dd, *J* = 14.9, 7.2 Hz, 1H), 3.25 (app. dd, *J* = 14.9, 9.1 Hz, 1H), 2.51 (app. td, *J* = 10.1, 3.7 Hz, 1H), 2.04 (m, 1H), 1.78 – 1.13 (m, 9H); $^{13}C\{^1H\}$ NMR (125 MHz, CD_2Cl_2): δ 184.1, 152.6, 150.0, 141.7, 138.9, 138.0, 132.3 (q, *J* = 33.1 Hz), 131.1, 129.1, 128.1, 125.7, 124.7 (q, *J* = 32.6), 123.9 (q, *J* = 272.6 Hz), 123.4, 122.7 (q, *J* = 271.1 Hz), 119.5, 118.5, 115.9 (quint, *J* = 3.8 Hz), 115.4, 113.7, 90.1, 66.1, 63.5, 56.4, 37.3, 35.2, 32.8, 25.0, 24.9; HRMS (ESI$^+$, TOF): m/z calcd for $[C_{32}H_{31}F_9N_5O_2S]^+$ 720.2049, found 720.2045, Δ = 0.6 ppm.

1-(2-(((1R,2R)-1-(3-((1S,2S)-2-aminocyclohexyl)thioureido)-2,3-dihydro-1H-inden-2-yl)oxy)-5-(trifluoromethyl)phenyl)-3-(3,5-bis(trifluoromethyl)phenyl)urea (**7**). The reaction performed using **4** (300 mg, 0.53 mmol, 100 mol-%) and (*S,S*)-**5** (121 mg, 1.06 mmol, 200 mol-%) using the procedure used for the preparation of **6**. The product was purified by flash chromatography (100:1:1 DCM:MeOH:Triethylamine) to afford **7** as off-white solid (290 mg, 76%). R_f (4% 7N NH_3/MeOH in DCM) = 0.45; mp 142−143 °C; $[\alpha]_D^{25\,°C}$ = −183.0 (*c* 1.0, DCM); IR (film, cm¬1): 3273, 2932, 2859, 1710, 1542, 1442, 1384, 1276, 1122, 681; ^1H NMR (500 MHz, CD_2Cl_2): δ 10.23 (s, 1H), 9.51 (s, 1H), 8.70 (d, *J* = 1.9 Hz, 1H), 8.53 (s, 1H), 8.19 (s, 2H), 7.52 (s, 1H), 7.31 – 7-24 (m, 5H), 7.08 (d, *J* = 8.4 Hz, 1H), 6.73 (d, *J* = 8.1 Hz, 1H), 6.07 (br s, 1H), 4.59 (q, *J* = 8.2 Hz, 1H), 3.67 (dd, *J* = 15.2, 7.4 Hz, 1H), 3.25 (dd, *J* = 15.1, 8.9 Hz, 1H), 3.08 (brs, 1H), 2.62 (td, *J* = 10.3, 3.5 Hz, 1H), 1.81 (app. d, J = 12.5 Hz, 1H), 1.75 – 1.63 (m, 5H), 1.21 – 1.07 (m, 4H); $^{13}C\{^1H\}$ NMR (125 MHz, CD_2Cl_2): δ 183.7, 152.5, 150.0, 141.7, 138.4, 137.9, 132.2 (q, *J* = 33.0 Hz), 131.1, 129.1, 127.9, 125.7, 124.8 (q, *J* = 271.6 Hz), 124.6 (q, *J* = 33.7 Hz), 123.9 (q, *J* = 272.7), 123.5, 119.4, 118.4, 115.7, 115.4, 113.9, 91.4, 66.3, 63.1, 56.4, 37.4, 35.1, 32.6, 24.9; HRMS (ESI$^+$, TOF): m/z calcd for $[C_{32}H_{31}F_9N_5O_2S]^+$ 720.2049, found 720.2062, Δ = −1.8 ppm.

1-(3,5-bis(trifluoromethyl)phenyl)-3-(2-(((1R,2R)-1-(3-((1R,2R)-2-(dimethylamino)cyclohexyl)thioureido)-2,3-dihydro-1H-inden-2-yl)oxy)-5-(trifluoromethyl)phenyl)urea (**2**). To a solution of compound **6** (200 mg, 0.28 mmol, 100 mol-%) in DCE (6 mL) was

added formaldehyde (38% CH_2O in water, 61 μL, 0.84 mmol, 300 mol-%) at rt. The reaction mixture was stirred at rt for 15 min after which $NaBH(OAc)_3$ (237 mg, 1.12 mmol, 400 mol-%) was added in one portion. The reaction mixture was stirred at rt for 4 h before sat. aq. $NaHCO_3$ (18 mL) was added. The mixture was allowed to stir for 15 min, and then the layers were separated. The aqueous layer was washed with DCM (3 × 18 mL). The combined organic extracts were dried over Na_2SO_4 and concentrated. Purification of the residue by flash chromatography (4% 7N NH_3/MeOH in DCM) afforded the desired product **2** as a pale crystalline solid (133 mg, 64%). Characterization data are in full agreement with our previous publication.[7c] ^{1}H NMR (500 MHz, CD_2Cl_2): δ 9.40 (b rs, 1H), 8.71 (s, 1H), 8.61 (s, 1H), 8.20 (s, 2H), 7.53 (s, 1H), 7.33 – 7-28 (m, 4H), 7.26 (dd, *J* = 8.4, 1.4 Hz, 1H), 7.09 (d, *J* = 8.4 Hz, 1H), 6.65 (s, 1H), 6.34 (brs, 1H), 4.46 (app. q, *J* = 8.1 Hz, 1H), 3.65 (dd, *J* = 14.6, 6.9 Hz, 1H), 3.49 (brs, 1H), 3.29 (dd, *J* = 14.6, 9.1 Hz, 1H), 2.31 (m, 1H), 2.21 (m, 1H), 1.93 (brs, 6H), 1.79 (m, 1H), 1.75 (m, 1H), 1.64 (brs, 1H), 1.27 (m, 1H), 1.16 – 1.12 (m, 3H); ^{13}C{^{1}H} NMR (75 MHz, CD_2Cl_2): δ 183.5, 152.6, 150.0, 141.8, 138.5, 138.1, 132.3 (q, *J* = 33.1 Hz), 129.2, 128.2, 125.8, 124.9 (q, *J* = 271.5 Hz), 124.9 (q, *J* = 31.7 Hz), 123.9 (q, *J* = 272.7 Hz), 119.5, 118.4, 115.7 (sept, *J* = 4.0 Hz), 115.4, 114.2, 90.9, 67.8, 65.6, 57.0, 40.1, 37.4, 33.8, 24.8 (2C), 22.6.

1-(3,5-bis(trifluoromethyl)phenyl)-3-(2-(((1R,2R)-1-(3-((1S,2S)-2-(dimethylamino)cyclohexyl)thioureido)-2,3-dihydro-1H-inden-2-yl)oxy)-5-(trifluoromethyl)phenyl)urea (**1**). The reaction was performed using **7** (187 mg, 0.28 mmol, 100 mol-%) utilizing the procedure used for the preparation of **2**. The product was purified by flash chromatography (4% 7N NH_3/MeOH in DCM) to afford **1** as a pale crystalline solid (145 mg, 75%). Characterization data are in full agreement with our previous publication.[7c] ^{1}H NMR (500 MHz, CD_2Cl_2): δ 9.61 (br s, 1H), 8.71 (s, 1H), 8.46 (s, 1H), 8.21 (s, 2H), 7.53 (s, 1H), 7.34 (m, 3H), 7.27 (d, *J* = 8.2 Hz, 2H), 7.09 (d, *J* = 8.4 Hz, 1H), 6.65 (brs, 1H), 6.00 (brs, 1H), 4.47 (app. q, *J* = 7.5 Hz, 1H), 3.65 (dd, *J* = 15.3, 7.6 Hz, 1H), 3.27 (app. dd, *J* = 15.3, 8.8 Hz, 2H), 2.34 (app. td, *J* = 10.5, 3.5 Hz, 1H), 2.02 (s, 6H), 1.79 (app. d, *J* = 11.2 Hz, 1H), 1.69 (m, 2H), 1.62 (m, 1H), 1.17 (m, 1H), 1.09 – 1.01 (m, 3H); ^{13}C{^{1}H} NMR (125 MHz, CD_2Cl_2): δ 184.3, 152.5, 150.0, 141.7, 138.4, 138.1, 132.3 (q, *J* = 33.1 Hz), 131.4, 129.2, 128.0, 125.8, 124.8 (q, *J* = 271.6 Hz), 124.8 (q, *J* = 32.4 Hz), 123.9 (q, *J* = 272.6 Hz), 123.3, 119.4 (app. q, *J* = 4.0 Hz), 118.4 (app. d, *J* = 3.0 Hz), 115.8 (quint, *J* = 3.9 Hz), 115.5, 114.7, 91.8, 68.3, 65.9, 57.2, 40.2, 37.5, 33.8, 24.8, 24.7, 22.5.

Typical Procedure for the Preparation of HCl Salts of Catalysts 1 and 2. To a solution of catalyst (10 mg, 0.013 mmol, 100 mol-%) in DCM (2 mL) was added aq. HCl (conc., 53 μL, 0.65 mmol, 5000 mol-%) at 0 °C. A white precipitate was immediately formed and the mixture was stirred for 5 min at rt. The solvent and the excess of HCl were removed carefully under reduced pressure.

All other Catalyst HX salts were prepared in an analogous manner except that for non-volatile acids, 110 mol-% of the corresponding acid was used. The crystalline salts were grown using diffusion method from a binary solvent mixture consisting of either cyclopentane, benzene or toluene (1st component) and dichloromethane (2nd component).

Note: The 2D NOESY spectrum of both HCl salts were measured with 500 MHz spectrometer at 30 °C (303 K). Both salts show some instability after 24 hours in CD_3CN. *ent*-**1**·HCl salt is only sparingly soluble in CD_3CN and as such the NMR sample was warmed up to 70 °C before the start of the measurement and then recooled to the probe temperature (303 K).

(1R,2R)-2-(3-((1R,2R)-2-(2-(3-(3,5-bis(trifluoromethyl)phenyl)ureido)-4-(trifluoromethyl)phenoxy)-2,3-dihydro-1H-inden-1-yl)thioureido)-N,N-dimethylcyclohexan-1-aminium chloride (**2**·HCl). ^{1}H NMR (500 MHz, CD_3CN): δ 11.10 (s, 1H), 9.28 (brs, 1H), 9.15 (s, 1H), 8.74 (s, 1H), 8.21 (s, 2H), 7.61 (br s, 1H), 7.57 (s, 1H), 7.32 – 7.24 (m, 5H), 7.17 (app. d, *J* = 8.3 Hz, 2H), 6.48 (t, *J* = 8.2 Hz, 1H), 5.29 (brs, 1H), 4.93 (brs, 1H), 3.63 (m, 2H), 2.83 (m, 1H), 2.78 (s, 3H), 2.77 (s, 3H), 2.24 (m, 1H), 2.08 (m, 1H), 1.90 (m, 1H), 1.80 (m, 1H), 1.59 – 1.49 (m, 2H), 1.41 – 1.26 (m, 2H); ^{13}C{^{1}H} NMR (125 MHz, CD_3CN): 182.8, 153.7, 149.3, 143.1, 140.1, 138.6, 132.4 (q, *J* = 32.9 Hz), 131.0, 129.6, 128.9, 128.7, 128.5, 128.4, 125.7 (q, *J* = 271.9), 126.3, 124.6, 124.5 (q, *J* = 272.0 Hz), 123.4 (q, *J* = 33.9 Hz) 119.9, 115.6, 112.6, 110.9, 84.2, 67.2, 63.2, 56.2, 42.9, 37.4, 36.2, 32.8, 25.1, 24.7, 23.3.

(1R,2R)-2-(3-((1S,2S)-2-(2-(3-(3,5-bis(trifluoromethyl)phenyl)ureido)-4-(trifluoromethyl)phenoxy)-2,3-dihydro-1H-inden-1-yl)thioureido)-N,N-dimethylcyclohexan-1-aminium chloride (*ent*-**1**·HCl)

^{1}H NMR (500 MHz, CD_3CN): 11.20 (s, 1H), 9.39 (s, 1H), 8.68 (s, 1H), 8.20 (s, 3H), 7.90 (br s, 1H), 7.59 (s, 1H), 7.38 – 7.28 (m, 4H), 7.24 (m, 1H), 6.78 (br s, 1H), 5.24 (m, 1H), 4.80 (m, 1H), 3.98 (m, 1H), 3.60 (dd, J_1 = 15.5, 7.1 Hz, 1H), 2.90 (d, *J* = 3.7 Hz, 3H), 2.83 (m, 1H), 2.79 (d, *J* = 4.3 Hz, 3H), 1.88 (m, 1H), 1.65 (app. d, *J* = 11.9 Hz, 1H), 1.47 (m, 1H), 1.42 (m, 1H), 1.26 – 1.12 (m, 3H), 0.75 (m, 1H); ^{13}C{^{1}H} NMR (125 MHz, CD_3CN): 183.1, 153.7, 149.0, 143.0, 139.5, 139.0, 132.6 (q, *J* = 32.9 Hz), 131.0, 129.9, 128.5, 126.2, 125.6 (q, *J* = 270.2 Hz), 125.1, 124.5 (q, *J* = 271.9 Hz,), 123.7 (q, *J* = 32.2 Hz), 120.1, 116.0, 115.7, 113.1, 110.9, 87.5, 67.4, 63.2, 56.1, 42.8, 37.8, 36.5, 32.9, 24.9, 24.7, 23.1.

Catalyst Solution Structure Elucidation. Catalyst **1** solution structure: The sample was prepared by dissolving catalyst **1** (10 mg, 0.0134 mmol, 100 mol %) in 0.6 mL DCM-d_2. The 2D NOESY spectrum was measured with 500 MHz spectrometer at 303 K. Catalyst **2** solution structure: The sample was prepared by dissolving catalyst **2** (10 mg, 0.0134 mmol, 100 mol %) in 0.6 mL DCM-d_2. The 2D NOESY spectrum was measured with 500 MHz spectrometer at 303 K.

Solution Structures of Catalysts Hexafluoroacetylacetonate salts. The sample of catalyst **1** hfacac salt was prepared by dissolving catalyst **1** (10 mg, 0.0134 mmol, 100 mol %) in 0.6 mL DCM-d_2 and hfacac (1.9 μL, 0.0134 mmol, 100 mol %) was subsequently added. The 2D NOESY spectrum was measured with 500 MHz spectrometer at 303 K. The sample of catalyst **2** hfacac salt was prepared by using the procedure used for the **1**·hfacac salt. The 2D NOESY spectrum was measured with 300 MHz spectrometer at 303 K.

Titration experiments. Titration of catalyst **1**·hfacac with tetra-n-butylammonium chloride (*n*-Bu_4NCl): Catalyst **1** (11.2 mg, 0.015 mmol, 100 mol %) was dissolved in CD_3CN (0.6 mL), hfacac (2.1 μL, 0.015 mmol, 100 mol %) was subsequently added and transferred to NMR tube. This solution was titrated with 0.5M solution of *n*-Bu_4NCl in CD_3CN. ^{1}H NMR (300 MHz) measurement was performed every 30 minutes after the addition of n-Bu_4NCl, insertion of the sample into the magnet, and initial shimming and receiver gain adjustment. All measurements were carried out at a probe temperature 303 K.

ASSOCIATED CONTENT

Supporting Information: Details of the X-ray structural characterization, and computational details: total energies and Cartesian coordinates for the considered stationary points. This material is available free of charge via the Internet at http://pubs.acs.org.

AUTHOR INFORMATION

Corresponding Author

*Petri.Pihko@jyu.fi

ACKNOWLEDGMENT

Financial support for this work was provided by the Academy of Finland (grants 297874 and 307624) and the Hungarian Scientific Research Fund (OTKA, grant K-112028). We thank Dr. Nicolas Probst for earlier synthetic and mechanistic efforts.

REFERENCES

(1) (a) Walsh, P. J.; Kozlowski, M. C. *Fundamentals of Asymmetric Catalysis*; University Science Books, Sausalito, CA, 2008. (b) Sunoj, R. B. Transition State Models for Understanding the Origin of Chiral Induction in Asymmetric Catalysis. *Acc. Chem. Res.* **2016**, *49*, 1019–1028.

(2) Harper, K. C.; Sigman, M. S. Predicting and Optimizing Asymmetric Catalyst Performance Using the Principles of Experimental Design and Steric Parameters. *PNAS*, **2011**, *108*, 2179–2183.

(3) Sharma, R.; Raudly, Z.; Miskei, M.; Fuxreiter, M. Fuzzy Complexes: Specific Binding without Complete Folding. *FEBS Letters*, **2015**, *589*, 2533–2542.

(4) Roca, M.; Messer, B.; Hilvert, D.; Warshel, A. On the Relationship between Folding and Chemical Landscapes in Enzyme Catalysis. *Proc. Natl. Acad. Sci.*, **2008**, *105*, 13877–13882.

(5) Petrović, D.; Risso, V. A.; Kamerlin, S. C. L.; Sanchez-Ruiz, J. M. Conformational Dynamics and Enzyme Evolution. *J. R. Soc. Interface*, **2018**, *15*, 1–18.

(6) (a) Hua, M.-Q.; Cui, H.-F.; Wang, L.; Nie, J.; Ma, J.-A. Reversal of Enantioselectivity by Tuning the Conformational Flexibility of Phase Transfer Catalysts. *Angew. Chem. Int. Ed.* **2010**, *49*, 2772–2776. (b) Sohtome, Y.; Tanaka, S.; Takada, K.; Yamaguchi, T.; Nagasawa, K. Solvent-Dependent Enantiodivergent Mannich-Type Reaction: Utilizing a Conformationally Flexible Guanidine/Bisthiourea Organocatalyst. *Angew. Chem. Int Ed.* **2010**, *49*, 9254–9257. (c) Metrano, A. J.; Abascal, N. C.; Mercado, B. Q.; Pulson, E. K.; Hurtley, A. E.; Miller, S. J. Diversity of Secondary Structure in Catalytic Peptides with β-Turn-Biased Sequences. *J. Am. Chem. Soc.* **2017**, *139*, 492–516. (d) Yan, X. C.; Metrano, A. J.; Robertson, M. J.; Abascal, N. C.; Tirado-Rives, J.; Miller, S. J.; Jorgensen, W. L. Molecular Dynamics Simulations of a Conformationally Mobile Peptide-Based Catalyst for Atroposelective Bromination. *ACS Catal.* **2018**, *8*, 9968–9979. (e) For a recent insightful review, see: Crawford, J. M.; Sigman, M. S. Conformational Dynamics in Asymmetric Catalysis: Is Catalyst Flexibility a Design Element? *Synthesis*, **2019**, *51*, 1021–1036.

(7) (a) Neuvonen, A. J.; Földes, T.; Madarász, Á.; Pápai, I.; Pihko, P. M. Organocatalysts Fold to Generate an Active Site Pocket for the Mannich Reaction. *ACS Catal.* **2017**, *7*, 3284–3294. (b) Neuvonen, A. J.; Pihko, P. M. Enantioselective Mannich Reaction of β-Keto Esters with Aromatic and Aliphatic Imines Using a Cooperatively Assisted Bifunctional Catalyst. *Org. Lett.* **2014**, *16*, 5152–5155. (c) Probst, N.; Madarász, Á.; Valkonen, A.; Pápai, I.; Rissanen, K.; Neuvonen, A.; Pihko, P. M. Cooperative Assistance in Bifunctional Organocatalysis: Enantioselective Mannich Reactions with Aliphatic and Aromatic Imines. *Angew. Chem. Int. Ed.* **2012**, *51*, 8495–8499. (d) The relative rates for catalysts **1** and **2** in the test reaction were estimated from the initial rates reported in ref 7c.

(8) For leading references to enantioselective Mannich reactions catalyzed by (thio)urea-tertiary amine catalysts, see: (a) Tillman, A. L.; Ye, J.; Dixon, D. J. Direct enantio- and diastereoselective Mannich reactions of malonate and β-keto esters with *N*-Boc and *N*-Cbz aldimines catalyzed by a bifunctional cinchonine derivative. *Chem. Commun.* **2006**, 1191–1193. (b) Song, J.; Wang, Y.; Deng, L. The Mannich Reaction of Malonates with Simple Imines Catalyzed by Bifunctional Cinchona Alkaloids: Enantioselective Synthesis of β-Amino Acids. *J. Am. Chem. Soc.* **2006**, *128*, 6048–6049. (c) Guo, Q.; Zhao, J. C.-G. Highly Enantioselective Three-Component Direct Mannich Reactions of Unfunctionalized Ketones Catalyzed by Bifunctional Organocatalysts. *Org. Lett.* **2013**, *15* , 508–510. (d) Kobayashi, S.; Mori, Y.; Fossey, J. S.; Salter, M. M. Catalytic Enantioselective Formation of C–C Bonds by Addition to Imines and Hydrazones: A Ten-Year Update. *Chem. Rev.* **2011**, *111*, 2626–2704.

(9) Jones, C. R.; Pantoş, G. D.; Morrison, A. J.; Smith, M. D. Plagiarizing Proteins: Enhancing Efficiency in Asymmetric Hydrogen-Bonding Catalysis through Positive Cooperativity. *Angew. Chem. Int. Ed.* **2009**, *48*, 7391–7394.

(10) (a) Supady, A.; Hecht, S.; Baldauf, C. About Underappreciated Yet Active Conformations of Thiourea Organocatalysts. *Org. Lett.* **2017**, *19*, 4199–4202. (b) Luchini, G.; Ascough, D. M. H.; Alegre-Requena, J. V.; Gouverneur, V.; Paton, R. S. Data-mining the Diaryl(thio)urea Conformational Landscape: Understanding the Contrasting Behavior of Ureas and Thioureas with Quantum Chemistry. *Tetrahedron*, **2019**, *75*, 697–702. (c) For a recent example of an anti-syn bisurea catalyst capable of binding fluoride, see: Pupo, G.; Ibba, F.; Ascough, D. M. H.; Vicini, A. C.; Ricci, P.; Christensen, K. E.; Pfeifer, L.; Morphy, J. R.; Brown, J. M.; Paton, R. S.; Gouverneur, V. Asymmetric nucleophilic fluorination under hydrogen bonding phase-transfer catalysis. *Science*, **2018**, *360*, 638–642. (d) Pupo, G.; Vicini, A. C.; Ascough, D. M. H.; Ibba, F.; Christensen, K. E.; Thompson, A. L.; Brown, J. M.; Paton, R. S.; Gouverneur, V. Hydrogen Bonding Phase-Transfer Catalysis with Potassium Fluoride: Enantioselective Synthesis of β-Fuoroamines. *J. Am. Chem. Soc.* **2019**, *141*, 2878–2883. (e) For a leading references to dimeric thiourea catalysts with halogen binding, see: Ford, D. D.; Lehnherr, D.; Kennedy, C. R.; Jacobsen, E. N. On- and Off-Cycle Catalyst Cooperativity in Anion-Binding Catalysis. *J. Am. Chem. Soc.* **2016**, *138*, 7860–7863. (f) Park, Y.; Harper, K. C.; Kuhl, N.; Kwan, E. E.; Liu, R. Y.; Jacobsen, E. N. Macrocyclic bis-thioureas catalyze stereospecific glycosylation reactions. *Science,* **2017**, *355*, 162–166.

(11) (a) Gale, P. A.; Howe, E. N. W.; Wu, X. Anion Receptor Chemistry. *Chem*, **2016**, *1*, 351–422. (b) Bregović, V. B.; Basarić, N.; Mlinarić-Majerski, K. Anion Binding with Urea and Thiourea Derivatives. *Coord. Chem. Rev.* **2015**, *295*, 80–124.

(12) All reported distances to hydrogens in the X-ray structures refer to calculated positions of the hydrogen atoms.

(13) Dunbrack Jr., R. L.; Karplus, M. Conformational Analysis of the Backbone-dependent Rotamer Preferences of Protein Sidechains. *Nature Structural Biology*, **1994**, *1*, 334–340.

(14) (a) Haushalter, K. A.; Lau, J.; Roberts, J. D. An NMR Investigation of the Effect of Hydrogen Bonding on the Rates of Rotation about the C–N Bonds in Urea and Thiourea. *J. Am. Chem. Soc.* **1996**, *118*, 8891–8896. (b) Chambers, C. C.; Archibong, E. F., Jalabameli, A.; Sullivan, R. H., Giesen, D. J.; Cramer, C. J., Truhlar, D. G. Quantum mechanical and ^{13}C dynamic NMR study of 1,3-dimethylthiourea conformational isomerizations. *J. Mol. Struct (Theochem)*, **1998**, *425*, 61–68.

(15) (a) Interestingly, thioureas appear to strongly prefer the *anti-anti* conformation when bound to chloride ions. based on a search of the CSD database. CSD: ConQuest V2.02 (2019); C. R. Groom, I. J. Bruno, M. P. Lightfoot and S. C. Ward, *Acta Cryst.* **2016**. *B72*, 171–179. Of the 98 hits found with thiourea N-H contacting the chloride ion, only a single example of an *anti-syn* or *syn-anti* conformation of a thiourea bound to chloride ion has been reported outside of these studies. See: (b) Soriano, M. L., Lenthall, J. T.; Anderson, K. W.; Smith, S. J.; Steed, J. W. Enhanced Anion Binding from Unusual Coordination Modes of Bis(thiourea) Ligands in Platinum Group Metal Complexes. *Chem. Eur. J.* **2010**, *16*, 10818–10831.

(16) For a review of fluoride sensors, see: Cametti, M.; Rissanen, K. Highlights on Contemporary Recognition and Sensing of Fluoride Anion in Solution and in the Solid State. *Chem. Soc. Rev.* **2013**, *42*, 2016–2038.

(17) In these experiments, *ent*-**1** was used due to temporary shortage of supply of catalyst **1**.